

Dynamic spin fluctuations and the bag mechanism of high- T_c superconductivity

J. R. Schrieffer, X. G. Wen, and S. C. Zhang

Institute for Theoretical Physics, University of California, Santa Barbara, California 93106

(Received 16 November 1988)

The spin-bag approach to the high-temperature superconductivity is presented in detail. The general argument that the local suppression of the electronic pseudogap leads to an attractive interaction of the quasiparticles is substantiated by the detailed calculation of the pairing potential mediated by the collective modes of the spin-density-wave background. In particular, the spin-wave spectrum, the sublattice magnetization, and the spectral distribution of the collective modes are studied within the random-phase approximation. In the low-doping limit, different shapes of the Fermi surface give rise to a superconducting gap which formally has d -wave- or p -wave-like symmetry, however the gap has no nodes on the Fermi surface. Therefore, the superconducting properties of our model are analogous to those of a conventional s -wave (i.e., nodeless) BCS superconductor. We also discuss possible bag effects in the large- U Hubbard model and in charge-density-wave systems. Finally, the relation of our work with other approaches and with experiment are discussed briefly.

I. INTRODUCTION

There is considerable experimental evidence that the properties of the newly discovered high-temperature oxide superconductors,¹ such as conventional superconductors, can be accounted for in terms of the pairing theory.² This evidence includes the factor of $2e$ occurring in the flux quantum and in the Josephson effect,³ as well as the electrodynamic and thermodynamic properties⁴ of these materials. While there remain experimental uncertainties, largely due to materials preparation problems, the central features of the data support the pairing approach. However, because of the short coherence length $\xi_{SC} \sim 12\text{--}20$ Å in the planes of the oxide superconductors, fluctuation effects are expected to be considerably larger than in conventional superconductors and a complete theory must include such effects.

The ingredients of the pairing theory are (1) the existence of spin- $\frac{1}{2}$ fermion quasiparticles in the normal phase of the material and (2) an attractive effective potential V between these quasiparticles. This attraction causes a cooperative phase transition to the superconducting state at a temperature T_c which is large compared to the temperature at which a single pair binds.

For conventional superconductors, V arises from the exchange of phonons between quasiparticles and is opposed by the screened Coulomb repulsion. Because of the retarded nature of the phonon interaction, the quasiparticles largely avoid the short-range Coulomb interaction yet benefit from the time-delayed phonon attraction. The phonon mechanism leads to condensation into a state having both orbital and spin angular momentum zero. In view of the reduced or negligible isotope effect in the layered oxide superconductors and the fact that the phonon mechanism is likely unable to account for transition temperatures in excess of 40–50 K, a new mechanism must be operating.

Other pairing interactions are observed, e.g., in superfluidity ³He, where the attraction is due to the ex-

change of spin fluctuations. Because of the smallness of the Fermi energy and the weakness of the pairing interaction, T_c is extremely small ($\sim 2 \times 10^{-3}$ K) for ³He. The condensation in this case consists of pairs having orbital and spin angular momentum one. It appears that spin fluctuations also lead to superconducting in the actinides such as UBe₁₃ and UPt₃, etc. Pairing in atomic nuclei arises from the attractive nucleon potential, with $T_c \sim 10^6$ K. Thus, the pairing theory has provided a framework which has successfully explained superconductivity in systems with widely different interactions involving energy scales spanning 13 orders of magnitude.

In oxide superconductors, the central theoretical questions are (1) what is the nature of the quasiparticle excitations in the normal phase and (2) what is the origin of the pairing interaction between these excitations? In a recent paper⁵ we have proposed that the normal-phase excitations are spin- $\frac{1}{2}$ fermions, corresponding to a hole surrounded by a region of reduced spin or charge-density-wave order. These “bag” excitations attract each other, as in the case of bipolarons. In the presence of the Fermi sea, the cooperative pairing condensation occurs at a temperature higher than that at which bipolaron formation occurs, leading to high-temperature superconductivity.

An important clue as to the nature of the normal and superconducting states of these oxides was recently provided by neutron⁶ and Raman⁷ scattering experiments. These data show that strong finite-range antiferromagnetic correlations exist in the superconducting phase and that long-range antiferromagnetic order occurs in the phase diagram near the superconducting phase. Thus it appears that antiferromagnetism and superconductivity are intimately related in these materials, in contrast to magnetism opposing superconductivity in conventional superconductors.

In La₂CuO₄, antiferromagnetic order occurs with a commensurate wave vector $Q = (\pi/a, \pi/b, 0)$, where Q is observed to remain commensurate for a finite level of doping. The sublattice magnetization is found to be large, of

order $\frac{1}{2}$ of a spin- $\frac{1}{2}$ per Cu site. This spin density appears to be largely on the copper atoms. These observations can be interpreted⁸ in terms of a Mott-Hubbard localized electron picture based on the electron-electron interaction U being assumed to be larger than the valence bandwidth W . Alternatively, a commensurate spin-density-wave interpretation based on an itinerant electron approach is also possible. Which picture is closer to reality is yet to be decided by experiment, although $U \sim W/2$ may be realized in nature.

Returning to the bag excitations, the internal structure of the quasiparticles as well as the pairing attraction arise from a common source—the local suppression of antiferromagnetic order in the vicinity of the quasiparticle. As discussed below for $U < W$, a hole injected into a spin-density-wave (SDW) system depresses the staggered magnetization S surrounding the hole, in a region whose size L and shape depend on the nature of the Fermi surface as well as the mean SDW amplitude. (A numerical study of the spin bag is performed in Ref. 9.) This region of depressed S provides a bag inside of which the hole is self-consistently trapped. The bag containing the hole moves as an entity and acts as a quasiparticle of spin- $\frac{1}{2}$ and charge e . It was shown⁵ that by temporarily sharing a common bag, two such quasiparticles interact via an attractive pairing potential, when proper account is taken of short-range correlations induced by the screened Coulomb potential.

In the opposite limit $U > W$,¹⁰ it has been recently shown by several authors that a similar result occurs if finite-range antiferromagnetic order exists. In essence, an added hole leads to a reduction of the local staggered order parameter by disordering the spins in the vicinity of the hole. Therefore, frustration disorders the spins inside the bag for $U > W$ while for $U < W$ the hole reduces the local Fermi-surface nesting and reduces the amplitude of the SDW inside the bag. The bag is formed by longitudinal (S_z) spin waves for $U < W$ and transverse spin waves for $U \gg W$. Presumably for $U \approx W$, both spin-disorder and spin-amplitude reduction play a role in dressing the quasiparticle and in producing the pairing attraction.

If local antiferromagnetic order were not to exist, it has been proposed that a local coupling of pairs of spins to total spin zero might occur, leading to a resonating-valence-bond-type (RVB) picture.¹¹ In this approach, the excitations are presumed to be spinless charge e bosons and chargeless spin- $\frac{1}{2}$ fermions, as in the quasi-one-dimensional conductor polyacetylene.¹² This scheme is distinct from the pairing theory since spinless charged particles rather than spin- $\frac{1}{2}$ charged particles are the building blocks of superconductivity, a crucial difference.

Finally, we note that the spin-bag approach discussed above may be extended to systems like $\text{Ba}(\text{Pb},\text{Bi})\text{O}_3$ (Ref. 13) which exhibit charge-density-wave-type (CDW) ordering. As in the SDW case, an added hole depresses the CDW order parameter in a region surrounding the hole whose size and shape depend on the Fermi surface and the CDW amplitude. Two such quasiparticles can interact via an attractive pairing potential as stated above. These charge-bag effects may also account for superconductivity in $(\text{Ba},\text{K})\text{BiO}_3$.¹³

In this paper we present a formalism which enables us to calculate the dynamical pairing potential between spin bags. The bag idea suggests that holes sharing a local depression of the SDW amplitude experience an attractive potential. It is therefore natural to consider the pairing interaction of the quasiparticles in the presence of the SDW background through the exchange of the collective amplitude fluctuation of the SDW condensate. Strictly speaking, such a calculation is only valid if there is infinitely long-ranged antiferromagnetic order present. While this does not happen at high doping concentrations in the superconducting regime, neutron scattering experiments give evidence for an antiferromagnetic correlation length of order 10–20 Å and fluctuations of energy $\omega_0 \leq 0.02$ eV. This local slowly fluctuating antiferromagnetic order still causes a SDW pseudogap to persist since $\omega_0 \ll 2\Delta \sim 1 - 2$ eV. In general, if the frequency scale associated with the fluctuation of the antiferromagnetically ordered domain is small compared with the pseudogap and if the length scale of the local antiferromagnetic order is large compared with the SDW coherence length, $\xi_{\text{SDW}} \equiv \hbar v_F / \Delta$, where v_F is the Fermi velocity in the absence of the SDW, the above starting point is qualitatively correct.

We note that the spin-bag approach is to be contrasted with conventional paramagnon theory.¹⁴ There one considers the pairing interaction between the electrons arising from the exchange of spin fluctuation above the normal state in the absence of the SDW. The interaction is purely repulsive in momentum space, peaked at the nesting wave vector \mathbf{Q} and leads to a weak d -wave pairing with four nodes on Fermi surface. What is neglected in this approach is the effect of the local antiferromagnetic order on the self-energy of the quasiparticles and, consequently, on their interaction.

In our approach, however, the effect of the antiferromagnetic background is built into the hole wave function so that the attractive interaction mediated by the collective amplitude fluctuation of the SDW leads to a nodeless pairing gap over the Fermi surface, although the formal symmetry can be of the p -wave or d -wave type, depending on the shape of the hole Fermi surface. In the case of the normal-state perturbation theory, nodes of the pairing gap are unavoidable since the Fermi surface is a continuous loop around $k=0$ where in the present case, with the SDW background present, the hole Fermi surface forms pockets at the magnetic zone boundary so that the nodes of the pairing gap can be avoided at the hole Fermi surface. The nodes of the pairing gap appear at the region of momentum space where there is a SDW gap, and has no effect on the superconducting properties. In building a theory for high- T_c superconductivity based on magnetic interaction, the main challenge is to find a consistent solution of the gap equation so that the pairing gap is nodeless over the Fermi surface, as most experiments indicate.⁴ The fact that our magnetic mechanism can indeed give rise to a nodeless pairing gap is quite remarkable.

The pairing interaction in the presence of the SDW has been studied extensively by Fenton in Ref. 15, in a somewhat different context. The relation between his approach and ours will be discussed at the end of Sec. III.

This paper is organized as follows: In Sec. II we review the basic formalism of the spin-density-wave approach to the Hubbard model and calculate the collective charge and spin-density fluctuation modes above the SDW condensate within the random-phase approximation. The sublattice magnetization is also obtained within the mean-field theory and with the first-order fluctuation effects included. In Sec. III, we present the detailed calculation of the pairing potential. The solution of the superconducting gap equation and the effect of fluctuations on the quasiparticle self-energy are presented in Sec. IV. Finally, we discuss our results and comment on charge bags in charge-density-wave systems in Sec. V.

II. COLLECTIVE MODES

Let us start by considering the two-dimensional Hubbard model¹⁶ on a square lattice

$$H = -t \sum_{\langle i,j \rangle} (c_{i,a}^\dagger c_{j,a} + \text{H.c.}) + U \sum_i n_{i\uparrow} n_{i\downarrow}, \quad (2.1)$$

where $\langle i,j \rangle$ denotes nearest neighbors. By transforming to momentum space, H can be expressed as

$$H = \sum_{k,a} \varepsilon_k c_{k,a}^\dagger c_{k,a} + \frac{U}{2} \frac{1}{N} \sum_{k,k',q} \sum_{a,a'} \delta_{a'a} \delta_{\beta'\beta} c_{k',a'}^\dagger c_{-k'+q,\beta'}^\dagger \times c_{-k+q,\beta} c_{k,a}, \quad (2.2)$$

where

$$\varepsilon_k = -2t(\cos k_x a + \cos k_y a), \quad (2.3)$$

α, β are the indices for spin quantization along the z direction, a is the lattice constant, and N is the total number of sites. All the momentum summations extend over the first Brillouin zone (Fig. 1).

The zeroth-order ($U=0$) ground state of H is defined by

$$\begin{aligned} c_{k\alpha} |0\rangle &= 0, \quad \varepsilon_k > E_F, \\ c_{k\alpha}^\dagger |0\rangle &= 0, \quad \varepsilon_k < E_F, \end{aligned} \quad (2.4)$$

$$\chi_0^{00}(q, \omega) = \frac{1}{N} \sum_k \left[-\frac{n_k(1-n_{k+q})}{\omega + \varepsilon_k - \varepsilon_{k+q} - i\delta} + \frac{n_{k+q}(1-n_k)}{\omega + \varepsilon_k - \varepsilon_{k+q} + i\delta} \right], \quad (2.8)$$

with $\chi_0^{ij}(q, \omega) = \delta^{ij} \chi_0^{00}(q, \omega)$ where n_k is the electron occupation number. In the presence of the interaction, these correlation functions can be calculated by the random-phase approximation (RPA), which, in graphical representation, sums over an infinite series of bubble graphs and ladder graphs (Fig. 2). This summation can be easily performed by using Dyson's equation. In the charge channel, one finds

$$\chi_{\text{RPA}}^{00}(q, \omega) = \frac{\chi_0^{00}(q, \omega)}{1 + U \chi_0^{00}(q, \omega)}, \quad (2.9)$$

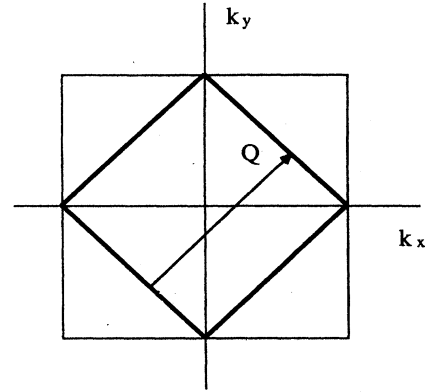


FIG. 1. The large square represents the first Brillouin zone; the small square represents the reduced Brillouin zone for the Bloch state in the SDW background, which is also the Fermi surface for free electrons at half-filling. Q is the nesting vector.

where E_F is the Fermi energy. At half-filling, the Fermi surface is a perfect square [the zero-energy contour of (2.3); see Fig. 1]. In this case, the ground state is unstable against spin-density fluctuations. To see this, let us look at the charge- and spin-density correlation functions defined by

$$\chi^{00}(q, t) = + \frac{i}{2N} \langle 0 | T \rho_q(t) \rho_{-q}(0) | 0 \rangle, \quad (2.5)$$

$$\chi^{ij}(q, t) = + \frac{i}{2N} \langle 0 | T S_q^i(t) S_{-q}^j(0) | 0 \rangle,$$

where

$$\rho_q = \sum_{k,a} c_{k+q,a}^\dagger c_{k,a} \quad (2.6)$$

is the charge-density operator and

$$S_q^i = \sum_{k,\alpha,\beta} c_{k+q,\alpha}^\dagger \sigma_{\alpha\beta}^i c_{k,\beta} \quad (2.7)$$

is the spin-density operator, with σ the Pauli matrices. In the absence of the interaction, these correlation functions are given by

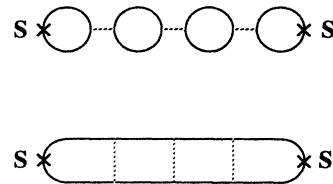


FIG. 2. The Feynman diagrams used in RPA to calculate χ_{RPA}^{00} and χ_{RPA}^{ij} . The single line represents the electron propagator in the normal state (no SDW). The dotted line represents the interaction U .

and in the spin channel, the result is

$$\chi_{\text{RPA}}^{ij}(q, \omega) = \frac{\chi_0^{00}(q, \omega)}{1 - U\chi_0^{00}(q, \omega)} \delta^{ij}. \quad (2.10)$$

At half-filling, the Fermi surface has the nesting property. Namely, there exists a vector \mathbf{Q} which connects opposite sides of the Fermi surface. This property leads to vanishing energy denominator $\varepsilon_k - \varepsilon_{k+Q}$ in $\chi_0^{00}(q=Q, \omega=0)$, and, consequently, one obtains a purely imaginary pole in $\chi_{\text{RPA}}^{ij}(Q, \omega)$ as a function of ω . In this case, $\chi_{\text{RPA}}^{ij}(Q, t) \sim \exp(\Omega_Q t)$ for large and positive t where Ω_Q is real and positive. This means that since the normal Fermi surface $|0\rangle$ defined by (4) is unstable and the true ground state $|\Omega\rangle$ is the one with a static spin-density wave present (for a review of the SDW formalism see Ref. 17). Without loss of generality, let us assume a SDW mean field to be polarized in the z direction

$$\langle \Omega | S_Q^z | \Omega \rangle \equiv \sum_k \langle \Omega | c_{k+Q, \alpha}^\dagger \sigma_{\alpha\alpha}^3 c_{k, \alpha'} | \Omega \rangle = SN, \quad (2.11)$$

where the variational parameter S will be determined later by a self-consistency condition. In the presence of this mean field, the Hartree-Fock factorized form of (2.2) is

$$H = \sum_{k, \alpha} \varepsilon_k c_{k, \alpha}^\dagger c_{k, \alpha} - \frac{US}{2} N \sum_{k, \alpha, \alpha'} c_{k+Q, \alpha}^\dagger \sigma_{\alpha\alpha'}^3 c_{k, \alpha'}. \quad (2.12)$$

This one-body Hamiltonian can be diagonalized by the transformation

$$\gamma_{k, \alpha}^c = u_k c_{k, \alpha} + v_k \sum_{\beta} (\sigma^3)_{\alpha\beta} c_{k+Q, \beta}, \quad (2.13a)$$

$$\gamma_{k, \alpha}^v = v_k c_{k, \alpha} - u_k \sum_{\beta} (\sigma^3)_{\alpha\beta} c_{k+Q, \beta}. \quad (2.13b)$$

To avoid double counting, k is restricted to the magnetic zone, i.e., one-half of the first Brillouin zone (see Fig. 1). The superscripts c and v refer to the conduction and the valence bands split by the exchange Bragg scattering from the SDW. The transformation amplitudes are

$$\begin{aligned} u_k &= \left[\frac{1}{2} \left(1 + \frac{\varepsilon_k}{E_k} \right) \right]^{1/2}, \\ v_k &= \left[\frac{1}{2} \left(1 - \frac{\varepsilon_k}{E_k} \right) \right]^{1/2}, \\ E_k &= (\varepsilon_k^2 + \Delta^2)^{1/2}, \\ \Delta &= -\frac{US}{2}, \end{aligned} \quad (2.14)$$

where Δ is the SDW energy gap parameter. The diagonalized Hamiltonian is given by

$$H = \sum_{k, \alpha} E_k (\gamma_{k\alpha}^c \gamma_{k\alpha}^c - \gamma_{k\alpha}^v \gamma_{k\alpha}^v), \quad (2.15)$$

where \sum_k means that the sum extends over the magnetic zone. The single-particle energy spectrum is given by

$\pm E_k$.

The SDW ground state $|\Omega\rangle$ for a half-filled band is defined by

$$\gamma_{k, \alpha}^{\dagger v} |\Omega\rangle = \gamma_{k, \alpha}^c |\Omega\rangle = 0. \quad (2.16)$$

Using this definition of the ground state $|\Omega\rangle$ in Eq. (2.11), one obtains a self-consistency condition determining the gap parameter Δ ,

$$\langle \Omega | S_Q^z | \Omega \rangle = -4 \sum_k' \frac{\Delta}{2E_k} = -\frac{2\Delta}{U} N \quad (2.17)$$

or

$$\frac{1}{N} \sum_k' \frac{1}{(\varepsilon_k^2 + \Delta^2)} = \frac{1}{U}. \quad (2.18)$$

Due to the singularity in the density of states at the Fermi surface, the solution of this gap equation for small U is given by

$$\Delta \sim t e^{-2\pi\sqrt{t/U}}, \quad (2.19)$$

while for $t \ll U$, $2\Delta = U$, the Mott-Hubbard gap.

Having discussed the single-particle spectrum in the SDW background, let us now turn our attention to the collective density fluctuation. To do that, we study the charge- and spin-density-correlation function as defined in Eq. (2.5) but the expectation value is taken with respect to the SDW ground state $|\Omega\rangle$ as defined in Eq. (2.16). Since there is a mean field which breaks the original crystal symmetry and doubles the unit-cell area, the correlation functions have off-diagonal terms in momentum space representation. These off-diagonal terms arise from the umklapp processes with respect to \mathbf{Q} . We therefore define the correlation functions in the presence of the SDW background by

$$\bar{\chi}^{00}(q, q', t) = \frac{i}{2N} \langle \Omega | T \rho_q(t) \rho_{-q'}(0) | \Omega \rangle, \quad (2.20)$$

$$\bar{\chi}^{ij}(q, q', t) = \frac{i}{2N} \langle \Omega | T S_q^i(t) S_{-q'}^j(0) | \Omega \rangle,$$

where ρ_q and S_q^i are given in Eqs. (2.6) and (2.7) and $|\Omega\rangle$ is defined by (2.16). To calculate these correlation functions in this mean-field approximation is straightforward. One transforms ρ_q and S_q^i into the γ representation by inverting Eq. (2.13). The time dependence of the γ operators is given simply by

$$\gamma_{k, \alpha}^c(t) = e^{-itE_k} \gamma_{k, \alpha}^c(0)$$

and

$$\gamma_{k, \alpha}^v(t) = e^{itE_k} \gamma_{k, \alpha}^v(0). \quad (2.21)$$

In evaluating the average, the only nonvanishing terms arise from the combinations such as

$$\langle \gamma_{k\alpha}^{\dagger v} \gamma_{p\beta}^c \gamma_{p'\beta'}^{\dagger v} \gamma_{k'\alpha'}^c \rangle = \delta(k-k') \delta(p-p') \delta_{\alpha\alpha'} \delta_{\beta\beta'} \quad (2.22)$$

and one obtains

$$\bar{\chi}_0^{00}(q, q'; \omega) = \delta(q-q') \bar{\chi}_0^{00}(q, \omega), \quad \bar{\chi}_0^{+-}(q, q'; \omega) = \delta(q-q') \bar{\chi}_0^{+-}(q, \omega) + \delta(q-q'+Q) \bar{\chi}_0^{+-}(q, \omega), \quad (2.23)$$

where

$$\bar{\chi}_0^{00}(q, \omega) = \bar{\chi}_0^{zz}(q, \omega) = -\frac{1}{2N} \sum_k' \left[1 - \frac{\varepsilon_k \varepsilon_{k+q} + \Delta^2}{E_k E_{k+q}} \right] \left[\frac{1}{\omega - E_{k+q} - E_k + i\delta} + \frac{1}{-\omega - E_{k+q} - E_k + i\delta} \right], \quad (2.24)$$

$$\bar{\chi}_0^{+-}(q, \omega) = -\frac{1}{2N} \sum_k' \left[1 - \frac{\varepsilon_k \varepsilon_{k+q} - \Delta^2}{E_k E_{k+q}} \right] \left[\frac{1}{\omega - E_{k+q} - E_k + i\delta} + \frac{1}{-\omega - E_{k+q} - E_k + i\delta} \right]. \quad (2.25)$$

The umklapp transverse susceptibility is given by

$$\bar{\chi}_Q^{+-}(q, \omega) = \frac{1}{2N} \sum_k' \frac{4\Delta}{E_k} \left[\frac{1}{\omega - E_{k+q} - E_k + i\delta} - \frac{1}{-\omega - E_{k+q} - E_k + i\delta} \right], \quad (2.26)$$

$$\bar{\chi}_0^{+-}(q, \omega) = \bar{\chi}_0^{-+}(q, \omega), \quad \bar{\chi}_Q^{+-} = -\bar{\chi}_Q^{-+}(q, \omega).$$

Equations (2.23)–(2.26) give the response functions in absence of the interaction. The RPA response functions can be obtained by solving the Dyson's equation (Fig. 3) and one finds

$$\bar{\chi}_{\text{RPA}}^{00}(q, q'; \omega) = \frac{\bar{\chi}_0^{00}(q, q'; \omega)}{1 + U\bar{\chi}_0^{zz}(q, \omega)}, \quad (2.27)$$

$$\bar{\chi}_{\text{RPA}}^{zz}(q, q'; \omega) = \frac{\bar{\chi}_0^{zz}(q, q'; \omega)}{1 - U\bar{\chi}_0^{zz}(q, \omega)}, \quad (2.28)$$

and

$$\bar{\chi}_{\text{RPA}}^{+-}(q, q'; \omega) = \sum_{q_1} \bar{\chi}_0^{+-}(q, q_1, \omega) [1 - U\bar{\chi}_0^{+-}(q_1, q'; \omega)]^{-1}. \quad (2.29)$$

$[1 - U\bar{\chi}_0^{+-}(q_1, q'; \omega)]^{-1}$ is a matrix inverse in momentum space and is given by

$$[1 - U\bar{\chi}_0^{+-}(q_1, q'; \omega)]^{-1} = \frac{[1 - U\bar{\chi}_0^{+-}(q_1 + Q, \omega)]\delta(q_1 - q') + U\bar{\chi}_Q^{+-}(q_1, \omega)\delta(q_1 - q' + Q)}{[1 - U\bar{\chi}_0^{+-}(q_1, \omega)][1 - U\bar{\chi}_0^{+-}(q_1 + Q, \omega)] - [U\bar{\chi}_Q^{+-}(q_1, \omega)]^2}. \quad (2.30)$$

From Eqs. (2.27)–(2.29) we observe a general feature of the spontaneous symmetry breaking: If the ground state is spin rotationally invariant, symmetry guarantees $\chi^{zz} = 2\chi^{+-}$. In our case, however, the ground state $|\Omega\rangle$ breaks the continuous spin rotational invariance of H and this relation no longer holds. As a result, χ^{+-} contains a gapless pole, as predicted by the Goldstone theorem. In fact, from (2.29) and (2.30) one can study the pole near $q = Q$, and find that the spin-wave spectrum is indeed gap-

less if

$$\frac{1}{N} \sum_k' \frac{1}{E_k} = \frac{1}{U}. \quad (2.31)$$

But (2.31) is identical to the gap Eq. (2.18) and this provides a nontrivial check of the self-consistency of the RPA calculation.

In order to find the spin-wave velocity v , we expand (2.29) and (2.30) for small $q - Q$ and small ω to locate the pole. Using the gap Eq. (2.18) we find

$$\bar{\chi}_{\text{RPA}}^{+-}(q, q', \omega) \cong + \frac{1}{U^2} \frac{(1/U - \Delta^2 x)\delta(q - q')}{(\omega \Delta x)^2 - [1/U - \Delta^2 x](t^2 y \delta q^2 - (\omega^2/4)x)}, \quad (2.32)$$

where

$$x \equiv \frac{1}{N} \sum_k' \frac{1}{E_k^3}, \quad y \equiv \frac{1}{N} \sum_k' \frac{\sin^2(k_x a)}{E_k^3}, \quad (2.33)$$

and $\delta q \equiv (q - Q)a$.

Equation (2.32) determines the spin-wave velocity for all values of t/U given by

$$v = \left[\frac{t^2 y (1/U - \Delta^2 x)}{\Delta^2 x^2 + (x/4)(1/U - \Delta^2 x)} \right]^{1/2}. \quad (2.34)$$

In the large limit, $x \rightarrow 1/2\Delta^3$, $y \rightarrow 1/4\Delta^3$, $2\Delta \rightarrow U$, and $1/U - \Delta^2 x \rightarrow 2t^2/\Delta^3$ as one can see directly by taking the large U solution of the gap Eq. (2.18). From (2.34) we

conclude that the spin-wave velocity in the large U limit is

$$v = \frac{1}{\sqrt{2}} J, \quad (2.35)$$

where $J = 4t^2/U$. This agrees exactly with Anderson's¹⁸ calculation of the spin-wave velocity of the $s = \frac{1}{2}$ Heisenberg model. In fact, with little more effort, one can work out the entire spin-wave spectrum in the large U limit for general q by expanding only to small $\omega \ll U$. We obtain $\omega_q = J(1 - \gamma_q^2)^{1/2}$ with $\gamma_q = \frac{1}{2}(\cos q_x a + \cos q_y a)$, again in exact agreement with the spin-wave spectrum of the Heisenberg model. In the small U limit, the solution of the gap equation is given by (2.19), and one sees explicitly that in this case, the spin-wave velocity v is of order ta .

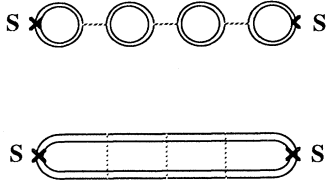


FIG. 3. The Feynman diagrams used to calculate $\bar{\chi}_{\text{RPA}}^{00}$ and $\bar{\chi}_{\text{RPA}}^U$ in the SDW background. The double line represents the electron propagator in presence of the SDW background.

By numerically solving the gap Eq. (2.18), we have determined the spin-wave velocity for all ranges of t/U from Eq. (2.32). The results are plotted in the Fig. 4.

Besides the spin-wave spectrum, the sublattice magnetization in the antiferromagnetic state is an important and experimentally accessible quantity. At large U , the effective Hamiltonian for the half-filled Hubbard model is known to be the Heisenberg antiferromagnetic Hamiltonian. The quantum-spin-wave fluctuations are known to reduce the mean-field sublattice magnetization of one μ_B per lattice site to about $0.6\mu_B$.^{18–20} It is very important to study the spin-wave-reduced sublattice magnetization in the present itinerant spin-density-wave approach as well. The mean-field approximation to the sublattice magnetization can be easily obtained by solving the gap Eq. (2.18) and using the definition (2.14), $|S| = 2\Delta/U$. The sublattice magnetization given by the numerical solution of the gap equation is plotted in Fig. 5. For small U the solution follows the behavior of Eq. (2.19), while for large $U, \Delta \gg \epsilon_k$, so that the left-hand side of Eq. (16) can be approximated by $1/2\Delta$, therefore, $\Delta \rightarrow U/2$ and $|S| \rightarrow 1$ just as in the localized limit.

To study the effect of fluctuations on the sublattice magnetization, we first derive a trivial identity

$$\begin{aligned} \langle S^i(x) \rangle &= \sum_{\alpha, \beta} \langle c_{\alpha}^{\dagger}(x, 0) \sigma_{\alpha\beta}^i c_{\beta}(x, 0) \rangle \\ &= -i \text{Tr} \sigma^i \mathbf{G}(x, 0^-; x, 0), \end{aligned} \quad (2.36)$$

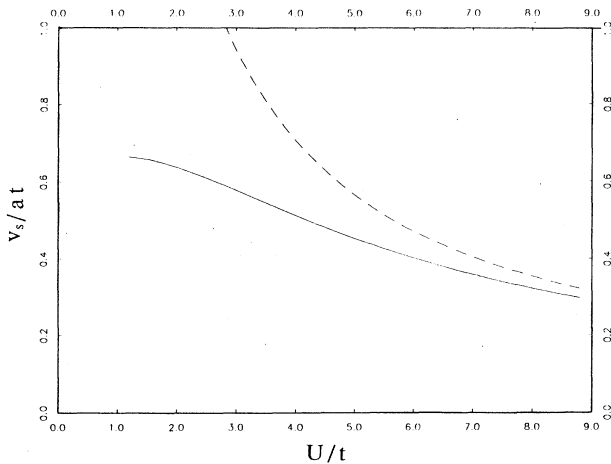


FIG. 4. The solid line represents the spin-wave velocity calculated using RPA. The dashed line plots $v_s/a = (1/\sqrt{2})J$ the spin-wave velocity expected for Heisenberg model.

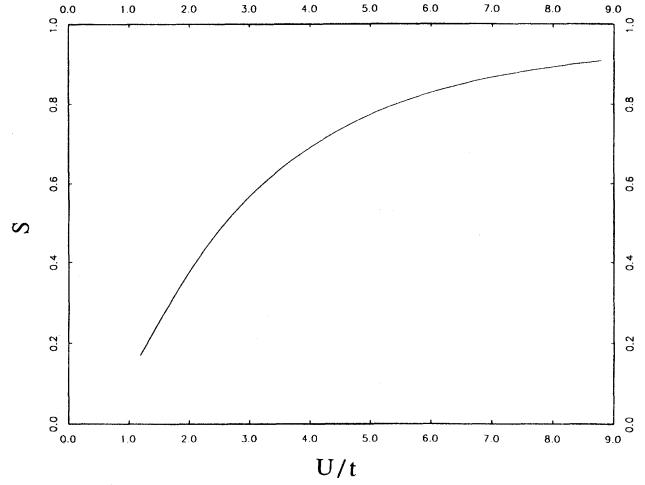


FIG. 5. The sublattice magnetization $S = 2\Delta/U$ obtained in mean-field theory.

where $\mathbf{G}_{\alpha\beta}(x_1 t_1; x_2 t_2) = -i \langle T c_{\alpha}(x_1 t_1) c_{\beta}^{\dagger}(x_2 t_2) \rangle$. Therefore the sublattice magnetization is given by

$$S = \frac{1}{N} \langle S_Q^z \rangle = -\frac{i}{N} \sum_k \int \frac{d\omega}{2\pi} \text{Tr} \sigma^3 \mathbf{G}(k, Q - k; \omega). \quad (2.37)$$

For the mean-field SDW vacuum $|\Omega\rangle$ as defined by Eq. (2.14), the one-particle Green's function is given by

$$G_{\alpha\beta}^0(p, p'; \omega) = \frac{(\omega + \epsilon_p) \delta_{\alpha\beta} \delta(p - p') + \Delta \sigma_{\alpha\beta}^3 \delta(p - p' + Q)}{\omega^2 - E_p^2 + i\delta}. \quad (2.38)$$

In this case,

$$\begin{aligned} S &= -\frac{i}{N} \sum_k \int \frac{d\omega}{2\pi} \text{Tr}(\sigma^3 \sigma^3) \frac{\Delta}{\omega^2 - E_k^2 + i\delta} \\ &= -\frac{\Delta}{N} \sum_k \frac{1}{E_k} = -\frac{2\Delta}{U}, \end{aligned} \quad (2.39)$$

just as given by Eq. (2.14).

In order to calculate the fluctuation effects on the sublattice magnetization, one simply has to calculate the self-energy correction to the one-particle Green's function. The self-energy matrix $\Sigma_{\alpha, \beta}(p, p', \omega)$ is approximated by the one-loop Feynman diagram (Fig. 6), where $\bar{\chi}_{\text{RPA}}^{00}$, $\bar{\chi}_{\text{RPA}}^{zz}$, and $\bar{\chi}_{\text{RPA}}^{+-}$ are given by Eqs. (2.27), (2.28), and (2.29), respectively. The full one-particle Green's function $\mathbf{G}_{\alpha\beta}(p, p', \omega)$ is then obtained by the Dyson's equation

$$\mathbf{G}_{\alpha\beta}^{-1}(p, p', \omega) = G_{\alpha\beta}^{0-1}(p, p', \omega) - \Sigma_{\alpha, \beta}(p, p', \omega). \quad (2.40)$$

We find that in the large U limit the charge fluctuations $\bar{\chi}_{\text{RPA}}^{00}$ and the amplitude spin fluctuations $\bar{\chi}_{\text{RPA}}^{zz}$ contribute

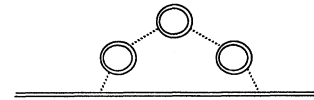


FIG. 6. The one-loop paramagnon correction to the self-energy of electron in the SDW state.

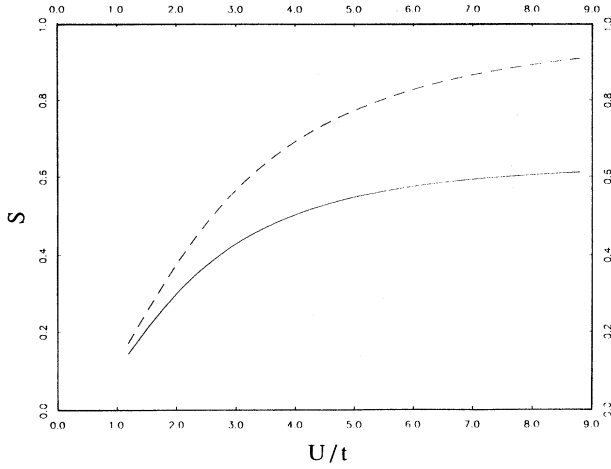


FIG. 7. The solid line represents the sublattice magnetization including the fluctuation effects. The dashed line is the mean-field result.

little to the reduction of the sublattice magnetization. In fact, their contribution to $\langle \delta S_z^2 \rangle / N$ is of order t^2/U^2 whereas the contribution from transverse spin fluctuations is of order 1. The numerical results for the transverse spin waves are summarized in Fig. 7. In the small U limit, the charge and the spin amplitude fluctuations are as important as the transverse one. However, in this case the effects of all fluctuations are small and $\langle S_z^2 \rangle / N$ is close to the mean-field value $2\Delta/U$. Therefore we expect the numerical result in Fig. 7 to be close to the true sublattice magnetization in both small and large U limit. It should also be good approximation for intermediate range of U . Actually, we can compare our RPA result with the recent computer simulations of Hirsch and Tang²⁰ and find fairly good agreements.

Neutron experiments seem to exclude the possibility of $S \lesssim 0.4$. This suggests that $\Delta/t \gtrsim 0.8$ or $U/t \gtrsim 2.9$ from our calculation. Within the range $0.8 \lesssim \Delta/t \lesssim 2.5$ (or $2.9 \lesssim U/t \lesssim 5.8$) the width of conduction band is larger than Δ and the itinerant electron picture describes the system more accurately than the localized electron picture.

In conclusion we find that the RPA calculations above the SDW background not only gives correct results in the small U limit, but also extrapolates sensibly to the large U limit, as reflected in the calculation of the spin-wave spectrum and the sublattice magnetization. In particular, these calculations clearly demonstrate the consistency of the itinerant picture with the neutron experiments.

III. PAIRING POTENTIAL

Having discussed both the single particle and the collective modes in the presence of the SDW background, we are now in the position to study the interactions of two holes doped into the half-filled band. The unperturbed states available to these holes are the eigenstates mean-field SDW Hamiltonian, the “ γ states” as given by Eq. (2.13). However, the interaction is easier to calculate as matrix elements between the original Bloch states, the “ c

states,” so that we calculate these interaction matrix elements first and then perform the transformation (2.13) to obtain the interaction matrix elements between the γ states.

Within the RPA, the interaction results from the exchange of the charge and spin collective modes given by (2.27)–(2.29) (Fig. 8). It is convenient to approximate the frequency dependence of each term in the interaction (0, z , \pm) by the static limit and a cutoff frequency, casting the results into an effective Hamiltonian. We find in the charge-fluctuation channel

$$H_c = \frac{1}{4N} \sum_{k,k',q} \sum_{\substack{a,a' \\ \beta,\beta'}} [2U - V_c(k-k')] \delta_{a'a} \delta_{\beta'\beta} \times c_{k'a'}^\dagger c_{-k'+q,\beta'}^\dagger c_{-k+q,\beta} c_{k,a}, \quad (3.1)$$

in the amplitude spin-fluctuation channel

$$H_z = -\frac{1}{4N} \sum_{k,k',q} \sum_{\substack{a,a' \\ \beta,\beta'}} V_z(k-k') \sigma_{a'a}^3 \sigma_{\beta'\beta}^3 \times c_{k'a'}^\dagger c_{-k'+q,\beta'}^\dagger c_{-k+q,\beta} c_{k,a}, \quad (3.2)$$

and in the orientational spin-fluctuation channel

$$H_{+-} = -\frac{1}{4N} \sum_{k,k',q} \sum_{\substack{a,a' \\ \beta,\beta'}} V_{+-}(k-k') \sigma_{a'a}^+ \sigma_{\beta'\beta}^- \times c_{k'a'}^\dagger c_{-k'+q,\beta'}^\dagger c_{-k+q,\beta} c_{k,a}, \quad (3.3)$$

where

$$\begin{aligned} V_c(q) &= \frac{U^2 \bar{\chi}_0^{00}(q)}{1 + U \bar{\chi}_0^{00}(q)}, \\ V_z(q) &= \frac{U^2 \bar{\chi}_0^{zz}(q)}{1 - U \bar{\chi}_0^{zz}(q)}, \\ V_{+-}(q) &= \frac{U^2 \bar{\chi}_0^{+-}(q)}{1 - U \bar{\chi}_0^{+-}(q)}. \end{aligned} \quad (3.4)$$

The total effective Hamiltonian is given by

$$H_{\text{eff}} = H_c + H_z + H_{+-} + H_{\uparrow-}. \quad (3.5)$$

Notice that we have explicitly included the original Hubbard interaction U in the charge channel. In Eqs. (3.1)–(3.3) $\bar{\chi}_0^{00}(q)$, $\bar{\chi}_0^{zz}(q)$, and $\bar{\chi}_0^{+-}(q)$ are the $\omega=0$ components of the dynamical susceptibilities defined in Eqs. (2.24) and (2.25). Since $\bar{\chi}_0^{+-}(q, \omega)$ is odd in ω and

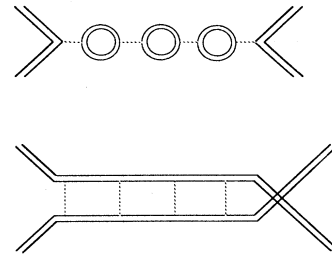


FIG. 8. The Feynman diagrams used in RPA to calculate the pairing potential in the SDW background.

vanishes for $\omega=0$, the momentum nonconserving term does not appear in H_{+-} .

We are now in the position to determine the matrix elements of the effective Hamiltonian in the γ -state basis and use them as the pairing potential. Transforming H_{eff} to the γ -state basis, one obtains the matrix elements for both intraband and interband transitions. At half-filling, the valence band is full and the conduction band is empty.

$$H_c \Rightarrow -\frac{1}{4N} \sum_{k,k'}' \sum_{\substack{a,a' \\ \beta,\beta'}} \{ [2U - V_c(k-k')] l^2(k,k') \delta_{a'a} \delta_{\beta\beta'} + [2U - V_c(k-k'+Q)] m^2(k,k') \sigma_{a'a}^3 \sigma_{\beta\beta'}^3 \} \gamma_{k,a}^+ \gamma_{-k,\beta}^+ \gamma_{-k,\beta}^- \gamma_{k,a}^-, \quad (3.6)$$

$$H_z \Rightarrow -\frac{1}{4N} \sum_{k,k'}' \sum_{\substack{a,a' \\ \beta,\beta'}} [V_z(k-k') l^2(k,k') \sigma_{a'a}^3 \sigma_{\beta\beta'}^3 + V_z(k-k'+Q) m^2(k,k') \delta_{a'a} \delta_{\beta\beta'}] \gamma_{k,a}^+ \gamma_{-k,\beta}^+ \gamma_{-k,\beta}^- \gamma_{k,a}^-, \quad (3.7)$$

$$H_{+-} \Rightarrow -\frac{1}{4N} \sum_{k,k'}' \sum_{\substack{a,a' \\ \beta,\beta'}} [V_{+-}(k-k') n^2(k,k') - V_{+-}(k-k'+Q) p^2(k,k')] \sigma_{a'a}^+ \sigma_{\beta\beta'}^- \gamma_{k,a}^+ \gamma_{-k,\beta}^+ \gamma_{-k,\beta}^- \gamma_{k,a}^-, \quad (3.8)$$

where

$$m(k,k') = u_k v_{k'} + v_k u_{k'}, \quad (3.9)$$

$$l(k,k') = u_k u_{k'} + v_k v_{k'}, \quad (3.10)$$

$$p(k,k') = u_k v_{k'} - v_k u_{k'}, \quad (3.11)$$

$$n(k,k') = u_k u_{k'} - v_k v_{k'}, \quad (3.12)$$

are the so-called coherence factors.

Equations (3.6)–(3.8) summarize the effective interactions in all channels between holes in the valence band, as calculated in the self-consistent random-phase approximation in the presence of the SDW background. We see H_{eff} has a fairly complicated structure. However, if we restrict ourselves to the weak doping limit, qualitative conclusions can be easily drawn. In this limit, the holes are concentrated at the top of the valence band, where $u_k^2 \approx v_k^2 \approx \frac{1}{2}$. One can therefore approximate the four coherence factors by $m(k,k') \approx l(k,k') \approx 1$, $p(k,k') \approx n(k,k') \approx 0$. An immediate consequence of this approximation is that these hole states are decoupled to the spin orientation fluctuations and the spin-flip scattering vanishes, i.e., $H_{+-} \approx 0$. Later we will see that only two states near the top of the valence band have a dominant contribution to the superconducting gap equation. The spin-orientation fluctuations are not important to the superconductivity in our model.

In the charge channel the pairing interaction between holes of opposite spin is given by

$$[2U - V_c(k-k')] - [2U - V_c(k-k'+Q)] \\ = -V_c(k-k') + V_c(k-k'+Q). \quad (3.13)$$

However, $V_c(q)$ is nothing but the original Coulomb interaction dressed by charge fluctuations. In contrast with the spin channel, the charge channel does not exhibit an instability and the renormalization effects are weak, with $V_c(q)$ having a weak momentum dependence. If we neglect the momentum dependence all together, (3.13) vanishes. This important result has a physical interpreta-

Weak doping removes electrons from the top of the valence band and it is these mobile holes which are responsible for the metallic behavior and superconductivity. Since the SDW gap 2Δ is large compared to the cutoff frequencies for the attractive parts of the pairing potential, one needs only retain the intra-valence-band matrix elements between hole pairs of opposite momentum, and we find

The states we are pairing are the eigenstates in the presence of the SDW, i.e., the γ states of Eq. (2.13). At the top of the valence band (or at the bottom of the conduction band) for which $u_k^2 \approx v_k^2 \approx \frac{1}{2}$, these states are superpositions of equal weight with states having momentum k and $k+Q$. In real space, if the wave function of an up-spin hole vanishes on the even sublattice due to destructive interference, between k and $k+Q$, the wave function of a down-spin hole vanishes on the odd sublattice. Therefore the matrix element of the on-site Coulomb repulsion vanishes due to the vanishingly small overlap of the up- and down-spin γ wave functions on the same site.

Now consider the interaction matrix element (3.7) in the amplitude fluctuation channel,

$$V_z(k-k') - V_z(k-k'+Q). \quad (3.14)$$

Unlike $V_c(q)$, $V_z(q)$, the longitudinal (non-spin-flip) exchange interaction is strongly enhanced by the magnetic fluctuations for $q \approx Q$, leading to a sharp momentum dependence. The reason for this is clear, $V_z(q)$ is proportional to the RPA magnetic susceptibility, which in the absence of SDW would diverge logarithmically at $q=Q$, indicating the antiferromagnetic instability. However, $V_z(q)$ is the RPA magnetic susceptibility in the presence of the mean-field SDW, and the system exhibits stable spin-wave excitations. For small Δ , a sharp peak of $V_z(q)$ is present at $q=Q$, with a width of the order of the inverse SDW coherence length $\xi_{\text{SDW}}^{-1} \sim \Delta/t$. From this structure of $V_z(q)$, one observes that the pairing interaction in the amplitude fluctuation channel (3.14) is strongly attractive for small momentum transfer and outweighs the interactions in all the other channels for holes near the gap edge. Therefore at relatively low doping the superconductivity is mainly due to the pairing potential in amplitude spin-fluctuation channel.

Strictly speaking, one can always work within the magnetic zone inside of which the γ states are originally defined. However, for most discussions, it is useful to work with the extended zone scheme. One can continu-

ously extend the definition of γ states outside of the magnetic zone using expression (2.13), since $\varepsilon_{k+Q} = -\varepsilon_k$ so that by (2.14), $u_{k+Q} = v_k$ and $v_{k+Q} = u_k$. Using this definition, we find

$$\gamma_{k,1}^{\uparrow} = -\gamma_{k+Q,1}^{\uparrow} \quad \text{and} \quad \gamma_{k,1}^{\downarrow} = \gamma_{k+Q,1}^{\downarrow}. \quad (3.15)$$

The first consequence of this definition is the fact that the pairing potential between holes with up and down spins are all antiperiodic functions in the magnetic zone, i.e., $V_{k,k'} = -V_{k+Q,k'} = -V_{k,k'+Q}$ as one sees directly from Eqs. (3.6)–(3.8). We note that the antiperiodicity of both the pairing potential and the basis states ensures that the total summands in the Hamiltonians are all periodic functions, and all the physical properties are invariant under the shifts of the origin of the magnetic zone. This unusual antiperiodicity arises from the fact that for a given k , $\gamma_{k,1}^{\uparrow}$ and $\gamma_{k,1}^{\downarrow}$ describe different orbital wave functions. One can avoid the antiperiodicity by working with a complex pairing potential or a discontinuous wave function, but for the purpose of solving the gap equation, our choice is the simplest. Another consequence of this choice is the fact that the superconducting order parameter

$$\Delta_k^{\text{SC}} = \sum_{k'} V_{kk'} \langle \gamma_{k',1}^{\uparrow} \gamma_{-k',1}^{\downarrow} \rangle$$

also turns out to be an antiperiodic function in the extended magnetic zone.

In the above discussion, we have limited ourself to the static limit. However, the energy cutoff of the pairing potential $V_{qq'}$ is an important parameter in solving the superconducting gap equation. In order to understand the energy cutoff, we study the spectral distribution of $\bar{\chi}_{\text{RPA}}^{zz}(q, \omega)$ for $\omega \neq 0$. Taking $t=1$, $\Delta=0.5$, and $U=2.28$, $\text{Re}\bar{\chi}_{\text{RPA}}^{zz}(Q, \omega)$ and $\text{Im}\bar{\chi}_{\text{RPA}}^{zz}(Q, \omega)$ are plotted as functions of ω in Fig. 9. We find a large portion of the spectral weight concentrated near $\omega=2\Delta$. Although no physical pole is found, the amplitude fluctuation of the SDW order parameter behaves approximately like a physical mode

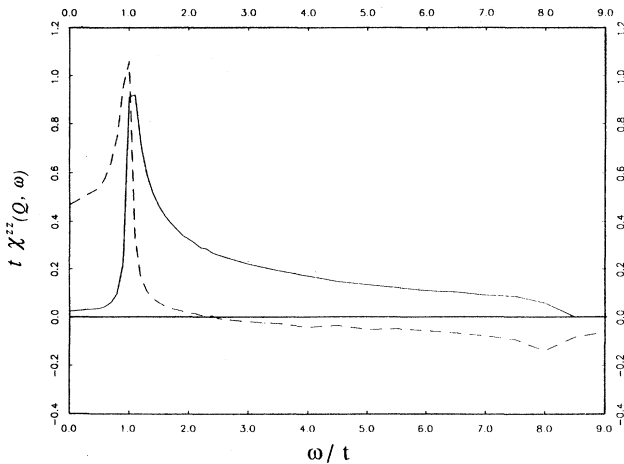


FIG. 9. The frequency dependence of the susceptibility $\bar{\chi}_{\text{RPA}}^{zz}(Q, \omega)$. The solid line is $\text{Im}\bar{\chi}_{\text{RPA}}^{zz}$. The dashed line is $\text{Re}\bar{\chi}_{\text{RPA}}^{zz}$.

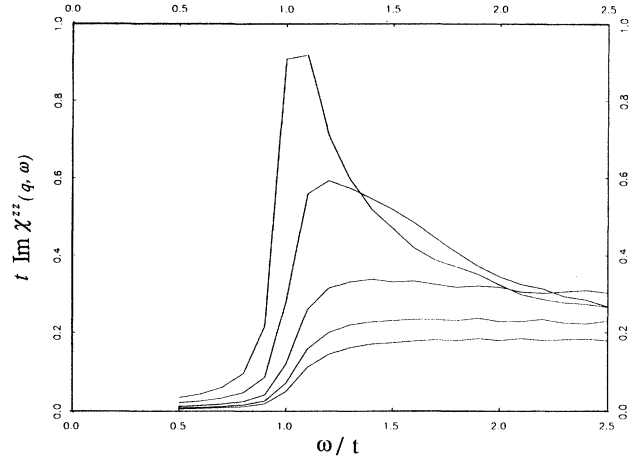


FIG. 10. The momentum dependence of $\bar{\chi}_{\text{RPA}}^{zz}(q, \omega)$ for ω near 2Δ . The five lines correspond to $|q-Q| = 0.1n|Q|$, $n=0, \dots, 4$, respectively.

with frequency $\omega \approx 2\Delta$. Away from the nesting vector $q=Q$, the spectral weight $\text{Im}\bar{\chi}_{\text{RPA}}^{zz}(q, \omega)$ near $\omega=2\Delta$ decreases rapidly (Fig. 10). Therefore it is reasonable to approximate $\bar{\chi}_{\text{RPA}}^{zz}(q, \omega)$ near $q=Q$ as

$$\bar{\chi}_{\text{RPA}}^{zz}(q, \omega) \approx \frac{-2\omega_a}{\omega^2 - \omega_a^2} A e^{-\lambda^2(q-Q)^2}, \quad (3.16)$$

$$\omega_a \approx 2\Delta.$$

From the numerical calculations we find for $t=1$, $\Delta=0.5$, and $U=2.28$,

$$\lambda \approx 0.9a,$$

$$A \approx 0.58,$$

and for $t=1$, $\Delta=1$, and $U=3.29$,

$$\lambda \approx 0.7a,$$

$$A \approx 0.45.$$

The dynamic pairing potential, between spin-up and spin-

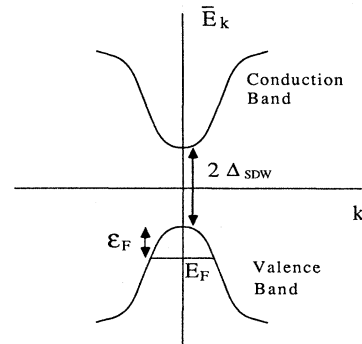


FIG. 11. The energy band of electrons in the SDW state. At finite doping ε_F is the Fermi energy of the holes.

down holes, is given by

$$-m^2(k, k')[U^2\bar{\chi}_{\text{RPA}}^{zz}(k-k'+Q, \omega)], \\ +l^2(k, k')[U^2\bar{\chi}_{\text{RPA}}^{zz}(k-k', \omega)]. \quad (3.17)$$

Therefore, if we use the effective Hamiltonian (3.7) to approximate the dynamic interaction given by (3.16) and (3.17), $V_z(k-k')$ in (3.7) may be taken to be

$$V_z(k-k') \approx U^2\bar{\chi}_{\text{RPA}}^{zz}(k-k', \omega=0)\Theta(\omega_a - |\bar{E}_k - E_F|) \\ \times \Theta(\omega_a - |\bar{E}_{k'} - E_F|), \quad (3.18)$$

where ω_a is the cutoff energy, E_F is the Fermi energy, \bar{E}_k

$$V_{kk'} = [-m^2(k, k')U^2\bar{\chi}_{\text{RPA}}^{zz}(k-k'+Q) + l^2(k, k')U^2\bar{\chi}_{\text{RPA}}^{zz}(k-k')] \Theta(\omega_a - |\bar{E}_k - E_F|) \Theta(\omega_a - |\bar{E}_{k'} - E_F|) \quad (3.20)$$

to be our pairing potential. For larger doping, we should include the scattering far away from the hole Fermi surface due to the interactions in the charge channel. Since there is no frequency cutoff for this interaction the charge channel potential leads to an effective pseudopotential acting in the region below ω_a which is much reduced in strength.

Let us conclude this section with a discussion of the relation between our work and that of Fenton.¹⁵ His main result is that the interaction entering the superconducting gap equation in the presence of the static SDW is the same as the interaction in the absence of the SDW, in apparent contradiction with our result. However, his conclusion is derived under the assumption that $u_k = u_k^*$, $v_k = -v_k^*$ so that $u_k v_k$ is purely imaginary. It is important to note that the phase of $u_k v_k$ is determined by the phase of the SDW relative to the underlying lattice. Choosing $u_k v_k$ to be purely imaginary corresponds to a SDW with spin-density peaked on the bonds and vanishing on the lattice sites. Therefore, it is quite conceivable that such a SDW does not modify the site interactions. However, in the presence case, the SDW results from a self-consistent solution of the Hubbard model and the spin-density necessarily has peaked on the sites. In this case $u_k v_k$ is real. As we showed in this section, the presence of such a SDW does in fact change the interaction in a dramatic fashion, producing an attractive potential. As one can see, we have fully included the interactions in all possible channels. The extra terms found by Fenton vanish identically in our case since u_k and v_k are both real.

IV. GAP EQUATION

Having completed our discussion of the pairing potential, we now proceed to solve the superconducting gap equation. At half-filling, there are no free carriers and the system is insulating due to the presence of the SDW band gap. With finite doping, the holes form a Fermi surface. Its shape in momentum space is most important for the nature of the superconducting gap.

One may notice that in the Hartree-Fock approxima-

tion, the energy spectrum of the electron (Fig. 11), and

$$\Theta(x) \equiv \begin{cases} 1, & x > 0, \\ 0, & x < 0. \end{cases} \quad (3.19)$$

Unlike $\bar{\chi}_{\text{RPA}}^{zz}(q, \omega)$, the spectral weight of $\bar{\chi}_{\text{RPA}}^{00}(q, \omega)$ is broadly distributed in the interval $-4t < \omega < 4t$ and has only a weak momentum dependence. Furthermore, according to our previous discussion, the pairing potential in the charge channel $V_{kk'}$ is ineffective for k and k' near the hole Fermi surface, since the holes are concentrated at the top of the valence band in the weak doping limit in which case spin-flip hole and spin-down hole occupy different sublattices. Therefore, in the following discussion, we shall simply take

tion, the single-electron energy spectrum $\pm E(k)$ is very special. For nearest-neighbor hopping the maximum of the valence-band energy $-E(k)$ is highly degenerate, consisting of two lines, $\tilde{k}_y=0$ and $\tilde{k}_x=0$ in the shifted magnetic Brillouin zone (Fig. 12). While this property is very unusual, one should realize that the degeneracy of the single-electron energies along the lines $\tilde{k}_x=0$ and $\tilde{k}_y=0$ is totally accidental and not guaranteed by symmetry. In reality, the single-electron energy $\bar{E}(\tilde{k}) = -E(\tilde{k}) + \Delta E(\tilde{k})$ for a valence-band electron has corrections $\Delta E(\tilde{k})$ arising from the higher-order corrections to the Hartree-Fock approximation, next-nearest-neighbor hopping and interactions between electrons on different sites, etc. For small concentrations of holes, the Fermi surface of Hartree-Fock spectrum $-E(\tilde{k})$ (Fig. 13) is highly sensitive to these perturbations. For example, if we add the energy correction $\Delta E(\tilde{k})$ which lifts the degeneracy such that the exact single-electron energy $\bar{E}(\tilde{k})$ has a single maximum at $\tilde{k}_x = \tilde{k}_y = 0$, then holes near $\tilde{k} = 0$ have the lowest energy and holes will concentrate in this vicinity. The resulting Fermi surface is a small circle around $\tilde{k} = 0$ (Figs. 12 and 14). If we assume, instead, that the corrected energy $\bar{E}(\tilde{k})$ has maxima at $(\tilde{k}_x, \tilde{k}_y) = (0, \pm\pi/\sqrt{2}a)$ and $(\pm\pi/\sqrt{2}a, 0)$ [$E(0, \pm\pi/\sqrt{2}a) = E(\pm\pi/\sqrt{2}a, 0)$ due to the x - y symmetry], holes tend to concentrate near

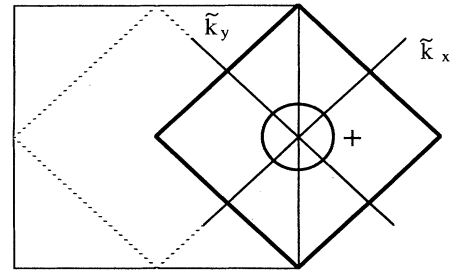


FIG. 12. The small square outlined by the bold line represents the shifted magnetic Brillouin zone. The circle is the Fermi surface at low doping, assuming the quasiparticle energy spectrum $\bar{E}(\tilde{k})$ satisfies $\bar{E}(\tilde{k}=0) < \bar{E}[\tilde{k}=(0, \pi/\sqrt{2}a)]$. The superconducting gap is positive along the Fermi surface.

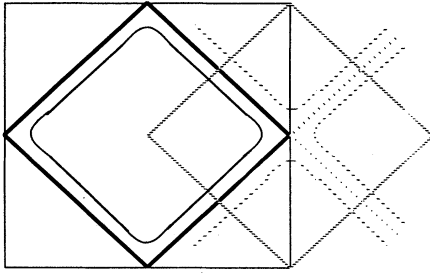


FIG. 13. The small square with the rounded corners is the Fermi surface for the mean-field energy spectrum E_k . The dotted lines are the Fermi surfaces in the shifted magnetic Brillouin zone.

$(0, \pm \pi/\sqrt{2}a)$ and $(\pm \pi/\sqrt{2}a, 0)$. For a small concentration of holes there are two separate Fermi surfaces as shown in Fig. 15. Therefore, at low doping the shape of the Fermi surface is not determined by $-E(\vec{k})$ but by the energy correction $\Delta E(\vec{k})$. In order to determine the shape of the Fermi surface, we must first evaluate $\Delta E(\vec{k})$.

Since $\Delta E(\vec{k})$ is composed of many contributions, it is very difficult to evaluate $\Delta E(\vec{k})$ reliably. For example, the one-loop spin-fluctuation self-energy correction (Fig. 6) tends to make valence electrons near $\vec{k}=0$ have higher energy. At $\vec{k}=0$, there is no quadratic term in the momentum expansion of the mean-field energy $E(k)$. However, the self-energy correction contributes to the quadratic term. Using the RPA susceptibility $\chi_{\vec{k}\vec{k}'}^{\text{RPA}}$ (3.16), we find the effective mass of holes at $\vec{k}=0$ is approximately given by $m^* \approx 11a^{-2}t^{-1} \approx 6m_e$ for $t=1$ eV, $a^2=12 \text{ \AA}^2$ for both $\Delta/t=0.5$ and $\Delta/t=1$. In the following we first discuss the case where the valence electrons at $\vec{k}=0$ have highest energy and the Fermi surface for a small concentration of holes is a small circle around $\vec{k}=0$, as shown in Fig. 14. The superconducting properties for the Fermi surface as shown in Fig. 15 will be discussed later.

The relevant Fermi energy in the problem is the Fermi

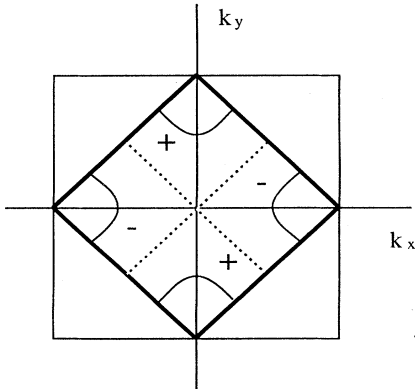


FIG. 14. The same Fermi surface as in Fig. 12 is represented in the (unshifted) magnetic Brillouin zone. The superconducting gap has alternating signs around the corners. The dotted lines are the node lines of the superconducting gap.

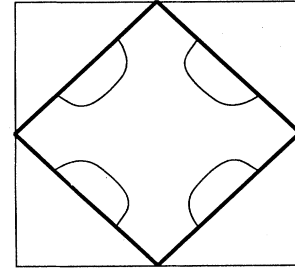


FIG. 15. The Fermi surface of electrons with spectrum $\bar{E}(k)$, assuming $\bar{E}[k=(0, \pi/a)] > \bar{E}[k=(\pi/2a, \pi/2a)]$.

energy of holes ε_F which is measured from the top of the valence band to the Fermi surface which has energy E_F (see Fig. 11). Thus $\varepsilon_F = \bar{E}(\vec{k}=0) - E_F$. At low doping, ε_F is less than the frequency cutoff of the pairing potential. Actually, $\varepsilon_F \approx 0.1$ eV for $m^* = 6m_e$ and hole density of 0.1 hole per site. Therefore, ε_F also serves as a frequency cutoff in the superconducting gap equation in addition to the frequency cutoff provided by the pairing potential. This leads to a superconducting gap and transition temperature which is rather sensitive to the doping concentration.

Due to the small frequency cutoff the empty conduction band can be ignored and the superconducting gap equation may be written as

$$\Delta_k^{\text{SC}} = - \sum_{k'} V_{kk'} \frac{\Delta_{k'}^{\text{SC}}}{2\bar{E}_{k'}} \quad (4.1)$$

where

$$\bar{E}_k = \sqrt{(\bar{E}_k - E_F)^2 + (\Delta_k^{\text{SC}})^2} \quad (4.2)$$

Strictly speaking the states very close to the bottom of the conduction band may contribute to the superconducting gap equation, since the frequency cutoff $\omega_a \approx 2\Delta$ is close to the gap between the conduction and valence bands. But such a contribution is small compared with that from the states in the valence band. Therefore the contribution from the conduction band can be safely ignored. Because of the antiperiodicity of the pairing potential

$$V_{k,k'} = -V_{k,k'+Q} = -V_{k+Q,k'} \quad (4.3)$$

one can easily check that the solution of the superconducting gap satisfies

$$\Delta_k^{\text{SC}} = -\Delta_{k+Q}^{\text{SC}} \quad (4.4)$$

Therefore Δ_k^{SC} must have lines of zeros in the magnetic zone. However, this does not necessarily imply that the total gap, antiferromagnetic-plus-superconducting, has zeros on the Fermi surface. This depends on the shape of the Fermi surface and the properties of the pairing potential. To see this, let us first look at the properties of the gap equation in the shifted zone where $\vec{k}=0$ is the center of the Fermi surface (see Fig. 12). In the case when the Fermi surface is a small circle around $\vec{k}=0$, only small momentum transfers are involved in scattering around the Fermi surface. Since the pairing potential is negative for

all small momentum transfers, a uniform superconducting gap near the Fermi surface is the solution. The lines of zeros of Δ_k^{SC} arising from (4.4) are on the magnetic zone boundary where a large SDW gap exists. Thus, Δ_k^{SC} is nonzero over the entire free Fermi surface and no power-law temperature dependence is expected.

One can also solve the gap equation directly in the original magnetic Brillouin zone where the Fermi surface is distributed at the corners (see Fig. 14). In this case, the superconducting gap Δ_k^{SC} has alternating signs as shown in Fig. 14. This is because of the strong positive peak of the pairing potential for momentum transfers near \mathbf{Q} . The resulting superconducting gaps for these two different choices of the magnetic Brillouin zone center can be mapped into each other by Eq. (4.4) (see Fig. 16). In both cases, the superconducting gap is nodeless at the Fermi surface since the SDW gap Δ preserves a gap when $\Delta^{\text{SC}} \rightarrow 0$. Thus, the zeros of superconducting gap are located in the regions of the Brillouin zone where there is no free Fermi surface.

To understand the symmetry of the superconducting order in SDW state, we calculate the superconducting order parameter in real space and find

$$\langle c_{i\uparrow} c_{j\downarrow} \rangle \propto \sum_k e^{ik(i-j)} [v_k + (-1)^i u_k] [v_k - (-1)^j u_k] \times \langle \gamma_{k\uparrow}^i \gamma_{-k\downarrow}^j \rangle, \quad (4.5)$$

where the summation extends over the magnetic zone in Fig. 1. $\langle \gamma_{k\uparrow}^i \gamma_{-k\downarrow}^j \rangle = \Delta_k^{\text{SC}} / 2E_k$ is nonzero only near the Fermi surfaces, i.e., near the four corners of the magnetic zone (Fig. 14) in low-doping limit. $\langle \gamma_{k\uparrow}^i \gamma_{-k\downarrow}^j \rangle$ has the same alternating signs around the four corners of the magnetic zone as Δ_k^{SC} . Since we are only interested in the symmetry properties of superconducting order parameter we may assume the order parameter to be proportioned to δ functions at the four corners and write

$$\langle \gamma_{k\uparrow}^i \gamma_{-k\downarrow}^j \rangle \propto \delta \left[k - \left(0, \frac{\pi}{a} \right) \right] + \delta \left[k + \left(0, \frac{\pi}{a} \right) \right] - \delta \left[k - \left(\frac{\pi}{a}, 0 \right) \right] - \delta \left[k + \left(\frac{\pi}{a}, 0 \right) \right]. \quad (4.6)$$

We find that in real space (4.6) gives

$$\langle c_{i\uparrow} c_{j\downarrow} \rangle \propto [1 + (-1)^i] \times [1 - (-1)^j] [(-1)^{i_x - j_x} - (-1)^{i_y - j_y}], \quad (4.7)$$

which is illustrated in Fig. 17.

From (4.7) we find that pairing is only between holes on different sublattices. This simply reflects the fact that at low doping the spin-up holes and spin-down holes live on different sublattices. Another property of the superconducting order parameter is that it changes sign under 90° rotation. Thus the symmetry of the order parameter resembles a d -wave pairing. However, as we emphasized earlier, there is no node on the Fermi surface in the low-doping limit and most properties of the superconductors are essentially the same as the conventional s -wave superconductor. But the sign change of the superconducting gap from corner to corner does have experimental significance. We expect that the superconducting state

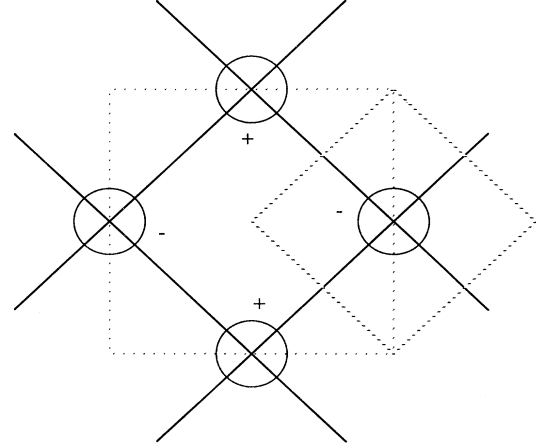


FIG. 16. The same Fermi surface and superconducting gap as in Figs. 12 and 14 is now represented in the repeated zone scheme.

can be suppressed by nonmagnetic impurities in the Cu-O plane similar to ordinary d -wave superconductivity.²¹

In order to estimate the magnitude of the superconducting gap, it is convenient to work in the shifted magnetic zone as shown in Fig. 12. In this case only the pairing potential for small momentum transfer is important and one can ignore the positive peak near $k - k' \sim Q$.

Note that in addition to the frequency cutoff, the pairing potential also has a momentum cutoff of order $1/\xi_{\text{SDW}}$. If the Fermi surface is small, i.e., the momentum transfer across the Fermi surface is less than $1/\xi_{\text{SDW}}$ we may rewrite the momentum cutoff as an effective frequency cutoff of order $1/2m^* \xi_{\text{SDW}}$ where m^* is the effective mass of holes. Therefore the effective frequency cutoff ω_0 is the smaller one of the two energies ω_a and $\frac{1}{2} m^* \xi_{\text{SDW}}$. In this case, we replace $V_{kk'}$ by

$$V_{kk'} \simeq -V_0 \Theta(\omega_0 - |\bar{E}_k - E_F|) \Theta(\omega_0 - |\bar{E}_{k'} - E_F|), \quad (4.8)$$

where $V_0 \simeq \frac{1}{4} [V_2(Q) - V_2(0)] \simeq \frac{1}{2} U^2 A / \omega_a$ [A is given in (3.16)].

At low doping since the Fermi surface is a small circle around $\tilde{k} = 0$, only the energy states near $\tilde{k} = 0$ are impor-

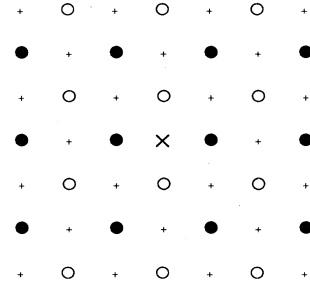


FIG. 17. The superconducting order parameter $\langle c_{i\uparrow} c_{j\downarrow} \rangle$ plotted as a function of j . \times marks the position of i , \circ represents a positive value, \bullet represents a negative value, and $+$ represents zero.

tant in solving the gap equation. Thus we can approximate \bar{E}_k by

$$\bar{E}_k \cong -\frac{1}{2m^*} \tilde{k}^2 + \text{const.} \quad (4.9)$$

near $\tilde{k}=0$. Now \tilde{E}_k becomes

$$\tilde{E}_k = \left[\left(\frac{\tilde{k}^2}{2m^*} - \varepsilon_F \right)^2 + \Delta_{SC}^2 \right]^{1/2}. \quad (4.10)$$

The superconducting gap equation can be easily solved. One finds

$$\ln \frac{(\omega_0^2 + \Delta_{SC}^2)^{1/2} + \omega_0}{\Delta_{SC}} + \ln \frac{(\varepsilon_F^2 + \Delta_{SC}^2)^{1/2} + \varepsilon_F}{\Delta_{SC}} = \frac{4\pi}{V_0 m^* a^2}, \quad (4.11)$$

which reduces to

$$\Delta_{SC} = 2\sqrt{\varepsilon_F \omega_0} \exp \left[-\frac{2\pi}{V_0 m^* a^2} \right] \quad (4.12)$$

in the limit $\Delta_{SC} \ll \varepsilon_F$ and ω_0 . Similarly, one finds the critical temperature

$$k_B T_c = 1.14 \sqrt{\varepsilon_F \omega_0} \exp \left[-\frac{2\pi}{V_0 m^* a^2} \right]. \quad (4.13)$$

The ratio $2\Delta_{SC}/T_c = 3.52$ is not changed by the appearance of the second frequency cutoff due to the small Fermi energy.

It is clear that the critical temperature T_c is very sensitive to the effective mass of the holes. Since $E(\tilde{k}) \sim (\tilde{k}_x^2 - \tilde{k}_y^2)^2$ near $\tilde{k}=0$ the quadratic term $\tilde{k}^2/2m^*$ in $\bar{E}(\tilde{k}) = -E(\tilde{k}) + \Delta E(\tilde{k})$ is completely due to the energy correction $\Delta E(\tilde{k})$. Therefore, the effective mass is determined by $\Delta E(\tilde{k})$ alone. Since we are not able to evaluate the energy correction $\Delta E(\tilde{k})$ reliably, we cannot estimate the effective mass m^* reliably from the first principle. Experiments suggest that $m^* \sim 5-10m_e$.

We would like to remark that the above analysis is correct only when $\Delta_{SC} \lesssim \varepsilon_F$. This is because the superconducting gap equation is derived using mean-field theory. The mean-field theory is correct only when there are many Cooper pairs in an area of the coherence length squared. In our case this leads to

$$n\xi_{SC}^2 \gtrsim 1, \quad (4.14)$$

where $\xi_{SC} = 2\pi v_F/\Delta_{SC}$ is the superconducting coherence length, v_F is the Fermi velocity, and n is the density of the holes. Using $v_F = (2\varepsilon_F/m^*)^{1/2}$ and $n = (2m^*/\pi)\varepsilon_F$, we find

$$n\xi_{SC}^2 = \frac{16\pi\varepsilon_F^2}{\Delta_{SC}^2} = \frac{4\pi\varepsilon_F}{\omega_0} \exp \left[-\frac{4\pi}{V_0 m^* a^2} \right].$$

This justifies that $\Delta_{SC} \lesssim \varepsilon_F$ is the correct condition for the mean-field theory to be valid. One may also consider the Cooper problem of two electrons binding above the rigid Fermi surface. The two electrons may form a bound state due to the attractive interaction between them. The bind-

ing energy is given by

$$\varepsilon_b = 2\omega_0 \exp \left[-\frac{4\pi}{V_0 m^* a^2} \right]. \quad (4.15)$$

Such a bound state can appear only when the temperature $T \lesssim \varepsilon_b$. Comparing ε_b with the superconducting transition temperature T_c , we find

$$\frac{\varepsilon_b}{T_c} \cong 2\sqrt{\omega_0/\varepsilon_F} \exp \left[-\frac{2\pi}{V_0 m^* a^2} \right] = \frac{\Delta_{SC}}{\varepsilon_F}. \quad (4.16)$$

Therefore, when $\Delta_{SC} \lesssim \varepsilon_F$, hence $\varepsilon_b \lesssim T_c$, the collective pairing of electrons (i.e., the superconducting transition) happens at a temperature higher than that at which two electrons can form a bound state in real space.

We would also like to remark that the spin-up and spin-down holes being paired are admixtures of singlet and triplet states. This is due to the fact that the spin-rotation symmetry is broken by the SDW mean-field vacuum and electron spin is not a good quantum number. This can be seen more clearly by considering the wave function of two paired electrons $\psi(k_1 a_1, k_2 a_2)$, where $a_i = \pm 1$ are the spin variables of electrons. The fact that the spin is not a good quantum number is reflected in that the wave function $\psi(k_1 a_1, k_2 a_2)$ cannot be rewritten in a factorized form $\psi_0(k_1, k_2) \psi_s(a_1, a_2)$, since the orbital wave functions of spin-up electrons and spin-down electrons are different, e.g., for the electrons near the top of the valence band, the wave functions vanish on the even lattice site for spin-up electrons while the wave functions for the spin-down electrons vanish on the odd site. Therefore, in our case the pairing wave function is the mixture of singlet and triplet spin states.

Above discussion we have discussed the superconducting properties for the Fermi surface in Fig. 14. With a little modification the above discussion also applies to the Fermi surface in Fig. 15. In this case the superconducting gaps have the sign indicated in Fig. 18. The superconducting gap still has no nodes on the Fermi surface. The 90° rotation is spontaneously broken in the superconducting state. The real-space superconducting order parameter

$$\langle c_{i\uparrow} c_{j\downarrow} \rangle \propto (i)^{i_x+i_y-j_x-j_y} [1+(-1)^{j_x-i_x}] [1-(-1)^{j_y-i_y}] \times [1+(-1)^i] [1-(-1)^j] \quad (4.17)$$

or

$$\langle c_{i\uparrow} c_{j\downarrow} \rangle \propto (i)^{i_x+i_y-j_x-j_y} [1-(-1)^{j_x-i_x}] [1+(-1)^{j_y-i_y}] \times [1+(-1)^i] [i-(-1)^j]$$

and is demonstrated in Fig. 19. The pairing wave function is odd under the 180° rotation which resembles a p -wave pairing.

We notice that in our d -wave-like superconducting state (for the Fermi surface in Fig. 14) the superconducting order parameter is a single complex scalar since the spacial rotation symmetry is broken by the lattice. But for our p -wave-like superconducting state for the Fermi surface in Fig. 15 the situation is very different. One may notice that there are two separated Fermi surfaces in Fig. 15 and

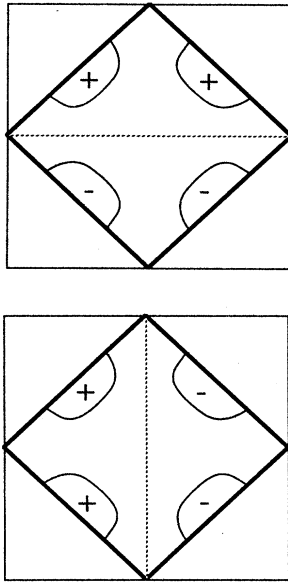


FIG. 18. The two possible sign configurations of the superconducting gaps for the Fermi surface in Fig. 15. The dotted lines are node lines of the superconducting gap.

the electrons on different Fermi surfaces have little interaction between them, at least in the low-doping limit. In this case the electrons near the two Fermi surfaces behave like two independent superfluids coupled by a weak Josephson-type coupling. Therefore, there are two complex superconducting order parameters $\phi_1 e^{i\theta_1}$ and $\phi_2 e^{i\theta_2}$ and the Ginzburg-Landau theory must be generalized to this case. The sum $\theta_1 + \theta_2$ of the two-phase-order

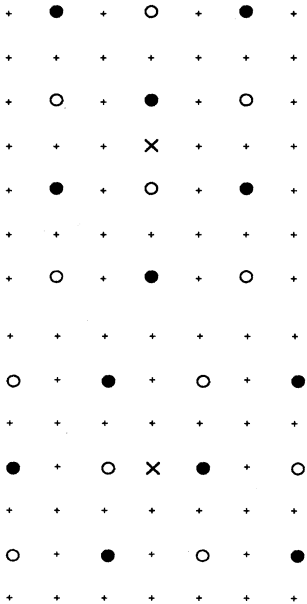


FIG. 19. The superconducting order parameters in real space for the two sign configurations in Fig. 18.

parameters is the Goldstone mode which is pushed to plasma frequency when the long-ranged Coloumb interaction is included, while the difference of the two-phase order parameter $\theta_1 - \theta_2$ remains to be a soft mode and is gapless in the limit when the two Fermi liquids decouple completely. The existence of this soft bosonic mode may have some important consequences on specific heat in the superconducting regime and the critical properties of the superconducting phase transition.

The superconducting state with *d*-wave-like symmetry is also obtained in Ref. 22. The pairing potential obtained there agrees with the one in Ref. 5 and in Sec. III of this paper. But as we have emphasized in Ref. 5 and in this paper, the superconducting state should be a nodeless one at least in the low-doping limit. A *p*-wave superconducting state in the presence of SDW is obtained in Ref. 23 in a somewhat different approach. Higher angular-momentum pairing with complex nodeless-pairing order parameter has been considered in Ref. 24.

V. DISCUSSION

In developing a theory of high-temperature oxide superconductivity, several fundamental issues must be addressed which ultimately will be answered by experiment. (1) Is the BCS formalism, involving the condensation of pairs of fermions, qualitatively correct or is a totally different approach necessary? (2) Are the observed finite-range strong spin correlations in the superconducting state crucial to the occurrence of high T_c , or is some other mechanism operative in these materials? (3) Is the itinerant electron or the Mott-Hubbard localized approach better suited to treating superconductivity in these materials? (4) Does the problem fundamentally involve one, two, or more bands or orbitals per unit cell?

There have been a number of Monte Carlo studies of the single-band Hubbard model.²⁵ The results of these studies show a suppression of the bare-particle-pairing susceptibility as the Hubbard interaction U is increased. However, when the renormalized one-particle Green's function is included,²⁶ a slight enhancement in the *d*-wave pairing susceptibility is found. This *d*-wave symmetry of the order parameter is consistent with our results, although for a detailed comparison more information on the nature of the hole Fermi surface must be extracted from the Monte Carlo studies.

A limiting feature of quantum Monte Carlo calculations is that they are carried out on relatively small lattices, e.g., 4×4 or 6×6 sites. For a doping level of $x = 0.1 - 0.15$ at which T_c is observed to peak, the system contains only 2-4 holes. It is unclear whether this small number can adequately describe the physics associated with the destruction of long-range spin order in the plane as well as the effects of pairing condensation. Furthermore, it is at present impossible to treat temperatures as low as the observed T_c in these materials. Another question is the role of finite-level spacing in these clusters compared to kT_c .

Finally, one knows that pairing occurs between the proper quasiparticles of the normal phase. The dressing of the bare particle to form such a quasiparticle, e.g., a

spin bag, is likely to lead to a small overlap between the bare particle states created by the operators used to define the gap parameter in the Monte Carlo studies and the quasiparticle states. If this overlap is indeed small, it is unclear if the Monte Carlo analysis is sufficiently accurate to properly recognize pairing were it to occur.

It would be helpful if the Monte Carlo studies were able to study the quasiparticles in the normal state as a prelude to studying superconductivity. In particular, it is important to investigate the correlation functions giving the spin distribution and the spin-spin correlations in the vicinity of a dynamic (versus localized) hole. The exact diagonalization performed by Dagotto *et al.*, clearly demonstrates the continuity of the spin-bag picture as a function of the coupling.²⁷

In our approach, we started from the single-band Hubbard model with the antibonding Cu $d_{x^2-y^2}$ and O p_σ orbitals being the relevant energy band. While this is an extremely simplified model, considering the complexity of these materials, we believe that this model incorporates the basic physics responsible for the high-temperature superconductivity. Within the weak to intermediate coupling regime we are considering, only the states close to the Fermi surface are important, while the details of the localized nature of the corresponding Wannier functions in the position space are less relevant. For a discussion between the relation of the one- and two-band model, see Zhang and Rice.²⁸

A more realistic model for the Cu-O plane of the high- T_c superconductors should involve three bands, from the bonding, nonbonding, and the antibonding combinations of the Cu $d_{x^2-y^2}$ and O p_σ orbitals. In the undoped samples, the bonding and the nonbonding bands are filled, while the antibonding band is half-filled. Due to the strong antiferromagnetic fluctuations, a SDW (pseudo) gap is opened at the Fermi surface. An important issue is whether the top of another energy band (e.g., the bonding or the nonbonding bands) happens to lie in the gap opened by the SDW. If this is the case, the doped hole will be at the top of this band rather than in the antibonding band and a genuine two-band model is needed to study the interaction of the holes and the antiferromagnetic fluctuations.²⁹ However, electron rather than hole-doped high- T_c materials have recently been synthesized, supporting the particle-hole symmetry characteristic of a one-band model. In general, the Fermi surface of the doped holes and the couplings to the spin fluctuations depend on which band is populated by the holes. However, our one-band spin-bag model and many other models involving two bands share the same physical feature that a doped hole destroys the antiferromagnetic order in its vicinity and thereby leads to an attractive interaction when two holes share the same region with the depressed antiferromagnetic order. Whether this attractive interaction can lead to a nodeless superconducting gap certainly depends on the shape of the hole Fermi surface. Within the two-band model, there are possibilities where the holes form pockets at the magnetic zone boundary,³⁰ just as the case of the one-band spin-bag model. In this case, it is likely that the superconducting gap is nonzero everywhere at the hole Fermi surface.

In this work we have assumed that strong spin correlations are intimately related to the large value of T_c in the cuprates. An important question is whether the spin order in the superconductor corresponds to local antiferromagnetic order or a coupling of pairs of spins to angular momentum zero as in the resonating-valence-bond-type state. Excitations in these two schemes are very different, the former leading to spin charge e fermions while the latter appears to support two types of excitations, spin- $\frac{1}{2}$ neutral fermions and spin-0 charge e bosons. We have taken the point of view that the spin correlations are locally antiferromagnetic in character so that the excitations are spin- $\frac{1}{2}$ charged fermions, consistent with a BCS pairing approach.

While the pairing theory is generally phrased in terms of a Fermi-liquid scheme based on an itinerant electron approach, the theory also applies to the holelike excitations in the Mott Hubbard regime if these excitations carry spin- $\frac{1}{2}$ and charge e , as in the weak-coupling regime. Several authors have discussed this possibility.¹⁰ As in the itinerant approach presented in this paper, the local antiferromagnetic order is reduced by the presence of a hole forming a bag or antiferromagnetic polaron type of excitation. It is possible that the bag simply changes in size as one goes from the weak-coupling (small U/t) to the strong-coupling (large U/t) limit, maintaining its spin and charge quantum numbers. In this case, one would expect that the correct physics of the materials could be treated starting from either limit.

Beginning with the itinerant scheme, we have shown that a hole in a commensurate spin-density-wave system preserves its spin and charge but clothes itself with a region of reduced antiferromagnetic order, the size of this region is given by the SDW coherence length $\xi_{SDW} \equiv \hbar v_F / \pi \Delta$. For typical values of the SDW gap $\Delta \sim 0.8$ eV and the Fermi velocity of the nonmagnetic phase $v_F \sim 5 \times 10^7$ cm/sec, ξ_{SDW} is of order $2a-3a$. The hole and its surrounding bag move as a quasiparticle whose mass we estimate to be of order $m_B \sim 6m_e$.

When a second quasiparticle is added, it is attracted to the other excitation, as worked out above. While this result is intuitively clear since the two holes can share (at least temporarily) a common bag thereby lowering their energy, this is in contrast with the corresponding situation in the absence of at least local antiferromagnetic order. In the nonmagnetic phase, one finds a repulsive interaction between quasiparticles in momentum space. Therefore, the existence of the SDW gap gives an increase of the hole energy which is reduced by the presence of a second hole, producing an effective attraction.

Whether these excitations actually bind in pairs or not in the weakly doped insulator is unclear, since the acceptor ions, e.g., the effective negatively charged Sr_x ions in the 2:1:4 material or the O ions in the 1:2:3 O_{6+x} material, may act as trapping centers for the positively charge bags.

In Fig. 20 a schematic phase diagram of the cuprate superconductors is shown as a function of the hole concentration x . The antiferromagnetic insulator is separated from the metallic region by an intermediate phase which has been described as spin-glass-like. One possible

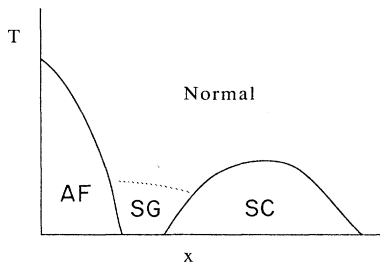


FIG. 20. A schematic phase diagram of the cuprate superconductors. AF, antiferromagnetic; SG, spin glass; SC, superconducting. x is the hole concentration.

scenario for this behavior is that the excitations are pinned by the charged acceptors in both the antiferromagnetically ordered phase as well as in the spin-glass phase. When the bag density increases beyond a critical value x_c , the exclusion principle increases the kinetic energy of the bags sufficiently to melt the glass, leading to a Fermi liquid of spin bags.

Regardless of the details of this intermediate phase, the bags are assumed to form a degenerate Fermi liquid in the metallic phase. While we have explicitly calculated the bag-bag interaction only in the long-range spin-ordered phase, it is plausible that a similar attraction occurs in the metallic phase if the range of spin order is larger than the bag size. It may be that this restriction is not essential for an attractive interaction to occur, a question we are now studying.

We have solved the BCS gap equation using the interaction between spin bags derived above. We find, as reported in our earlier publication, that Δ_k^{SC} is nodeless over the Fermi surface. However, the traditional characterization of Δ_k^{SC} as s , p , or d like is not an invariant concept in the presence of strong-band-structure effects, since for ex-

ample one can transform from d -like to s -like behavior by shifting the origin of k space, as shown above (see Figs. 12 and 14). The essential point is that the magnitude of Δ_k^{SC} is found to be nonzero at all points of the Fermi surface and no power-law temperature dependence is expected as in conventional $l > 0$ superconductors. The nodeless properties of the superconducting state have been observed in many experiments.⁴

Analogous bag effects may be operating in CDW superconductors, like $\text{Ba}(\text{Pb,Bi})\text{O}_3$ and possibly $(\text{Ba,K})\text{BiO}_3$.¹³ It is known that CDW correlations occur in the former and lead to a pseudogap. We have found that charge-bags form in this case as well and such bags are attractive, however the charge fluctuations are coupled to phonons leading to a partial isotope effect.

A number of questions remain to be resolved regarding the bag approach. (1) Are the spin and charge of the excitations correctly predicted in the antiferromagnetic insulator and in the metallic phase? (2) What is the actual shape of the Fermi surface in the metal and is the pairing-order parameter free of nodes on the Fermi surface? (3) What is the influence of quantum fluctuations in the superconducting properties? (4) Can the bag approach account for the general experimental facts which are not subject to materials difficulties? Hopefully, these issues will be clarified in the foreseeable future.

ACKNOWLEDGMENTS

We would like to acknowledge helpful discussions with E. Abrahams, S. Chakravaty, S. Kivelson, H. Nakanishi, D. J. Scalapino, and K. Schonhammer. This work was supported in part (J.R.S. and S.C.Z.) by the National Science Foundation Grant No. DMR 85-17276 and also (X.G.W.) No. PHY82-17853, supplemented by funds from the National Aeronautics and Space Administration.

- ¹J. G. Bednorz and K. A. Müller, *Z. Phys. B* **64**, 189 (1986); C. W. Chu *et al.*, *Phys. Rev. Lett.* **58**, 405 (1987).
- ²J. Bardeen, L. N. Cooper, and J. R. Schrieffer, *Phys. Rev.* **108**, 1175 (1957).
- ³P. L. Gammel *et al.*, *Phys. Rev. Lett.* **59**, 2592 (1987); C. E. Gough *et al.*, *Nature (London)* **326**, 855 (1987); T. Witt, *Phys. Rev. Lett.* **61**, 1423 (1988).
- ⁴Y. J. Uemura *et al.*, *Phys. Rev. B* **38**, 909 (1988); D. R. Harshman *et al.*, *ibid.* **36**, 2386 (1987); S. E. Inderhees *et al.*, *ibid.* **36**, 2401 (1987); G. A. Thomas *et al.*, *Phys. Rev. Lett.* **61**, 1313 (1988).
- ⁵J. R. Schrieffer, X. G. Wen, and S. C. Zhang, *Phys. Rev. Lett.* **60**, 944 (1988).
- ⁶G. Shirane *et al.*, *Phys. Rev. Lett.* **59**, 1613 (1987); J. Transquada *et al.*, *ibid.* **60**, 156 (1988).
- ⁷K. B. Lyons *et al.*, *Phys. Rev. B* **37**, 2353 (1988); K. B. Lyons *et al.*, *Phys. Rev. Lett.* **60**, 732 (1988).
- ⁸S. Chakravaty, B. I. Halperin, and D. R. Nelson, *Phys. Rev. Lett.* **60**, 1057 (1988).
- ⁹W. P. Su, *Phys. Rev. B* **37**, 9904 (1988).
- ¹⁰Y. Nagaoka, *Phys. Rev.* **147**, 392 (1966); W. F. Brinkman and T. M. Rice, *Phys. Rev. B* **2**, 1324 (1970); B. Shraiman and E. Siggia, *Phys. Rev. Lett.* **60**, 740 (1988); S. Schmitt-

- Rink, C. M. Varma, and A. E. Ruckenstein, *ibid.* **60**, 2793 (1988); S. A. Trugman, *Phys. Rev. B* **37**, 1597 (1988); C. L. Kane, P. A. Lee, and N. Reed (unpublished); A. Aharony *et al.*, *Phys. Rev. Lett.* **60**, 1330 (1988).
- ¹¹P. W. Anderson, *Science* **235**, 1196 (1987); P. W. Anderson, G. Baskaran, Z. Zou, and T. Hsu, *Phys. Rev. Lett.* **58**, 2790 (1987); S. A. Kivelson, D. S. Rokhsar, and J. P. Sethna, *Phys. Rev. B* **35**, 8865 (1987); R. B. Laughlin, *Phys. Rev. Lett.* **60**, 2677 (1988).
- ¹²W. P. Su, J. R. Schrieffer, and A. J. Heeger, *Phys. Rev. B* **22**, 2099 (1980).
- ¹³A. W. Sleight, J. L. Gillson, and P. E. Bierstedt, *Solid State Commun.* **17**, 27 (1975); R. J. Cara *et al.*, *Nature (London)* **332**, 814 (1988).
- ¹⁴K. Miyake, S. Schmitt-Rink, and C. M. Varma, *Phys. Rev. B* **34**, 6554 (1986); D. J. Scalapino, E. Loh, Jr., and J. E. Hirsch, *ibid.* **34**, 8190 (1986); D. J. Scalapino and E. Loh, Jr., *ibid.* **35**, 6694 (1987).
- ¹⁵E. W. Fenton, *Solid State Commun.* **65**, 343 (1988), and references therein.
- ¹⁶J. Hubbard, *Proc. R. Soc. London, Ser. A* **276**, 283 (1963); see also J. E. Hirsch, *Phys. Rev. B* **31**, 4403 (1985).
- ¹⁷E. Fawcett, *Rev. Mod. Phys.* **60**, 209 (1988).

- ¹⁸P. W. Anderson, Phys. Rev. **86**, 694 (1952).
- ¹⁹J. D. Reger and A. P. Young, Phys. Rev. B **37**, 5978 (1988).
- ²⁰J. E. Hirsch and S. Tang (unpublished).
- ²¹We note that a recent experiment [Ong (private communication)] indicates that Z_n doping in Cu-O plane destroys the superconductivity in both the 2:1:4 and the 1:2:3 materials.
- ²²H. Y. Chou and E. J. Mele, Phys. Rev. B **38**, 4540 (1988); Z. Y. Weng, T. K. Lee, and C. S. Ting (unpublished); G. Vignale and K. S. Singwi (unpublished).
- ²³Z. B. Su *et al.*, Z. Phys. B **70**, 131 (1988).
- ²⁴W. Harrison, Phys. Rev. B **38**, 270 (1988).
- ²⁵J. E. Hirsch, Phys. Rev. B **31**, 4403 (1985); J. E. Hirsch and H. Q. Lin, *ibid.* **37**, 5070 (1988).
- ²⁶S. R. White *et al.*, Phys. Rev. B (to be published).
- ²⁷E. Dagotto *et al.* (unpublished).
- ²⁸F. C. Zhang and T. M. Rice, Phys. Rev. B **37**, 3759 (1988).
- ²⁹V. J. Emery, Phys. Rev. Lett. **58**, 2794 (1987); J. E. Hirsch, *ibid.* **59**, 228 (1987); R. J. Birgeneau, M. A. Kastner, and A. Aharony, Z. Phys. B **71**, 57 (1988); J. Zaanen and A. Oles, Phys. Rev. B **37**, 9423 (1988).
- ³⁰L. Roth, Phys. Rev. Lett. **60**, 379 (1988); R. J. Gooding, D. F. Frenkel, B. I. Shraiman, and E. D. Siggia (unpublished).